Dislocation Structure and Mobility in hcp ^{4}He

Edgar Josué Landinez Borda, Wei Cai, and Maurice de Koning

Phys. Rev. Lett. **117**, 045301 — Published 20 July 2016

DOI: 10.1103/PhysRevLett.117.045301

Dislocation Structure and Mobility in hcp ^{4}He

Edgar Josué Landinez Borda,[1,*] Wei Cai,[2,†] and Maurice de Koning[3,‡]

[1] *Lawrence Livermore National Laboratory, 7000 East Ave, Livermore, CA 94550*
[2] *Department of Mechanical Engineering, Stanford University, Stanford, CA 94305-4040*
[3] *Instituto de Física "Gleb Wataghin", Universidade Estadual de Campinas, UNICAMP, 13083-859, Campinas, São Paulo, Brazil*

(Dated: July 5, 2016)

Using path-integral Monte Carlo simulations we assess the core structure and mobility of the screw and edge basal-plane dislocations in hcp ^{4}He. Our findings provide key insight into recent interpretations of giant plasticity and mass flow junction experiments. First, both dislocations are dissociated into nonsuperfluid Shockley partial dislocations separated by ribbons of stacking fault, suggesting that they are unlikely to act as 1D channels that may display Lüttinger-liquid-like behavior. Second, the centroid positions of the partial cores are found to fluctuate substantially, even in the absence of applied shear stresses. This implies that the lattice resistance to motion of the partial dislocations is negligible, consistent with the recent experimental observations of giant plasticity. Further results indicate that both the structure of the partial cores as well as zero-point fluctuations play a role in this extreme mobility.

Although the possible existence of superfluidity in hcp ^{4}He [1, 2] remains elusive [3], recent experiments on this archetypal bosonic quantum solid continue to pose questions that remain unresolved. Among these are the observations of giant plasticity [4–6] and the apparent superfluidlike mass transport [7–11]. Although the observed phenomena in the several experimental setups are quite different, the interpretation of the results has invariably involved the role of dislocations, the line defects that mediate plastic deformation in crystalline solids [12, 13]. In particular, both the core structure as well as their mobility have been involved in the discussion. While the giant plasticity has been interpreted in terms of virtually resistance-less motion of dislocations in the basal plane of hcp ^{4}He [4–6], the apparent superfluid mass transport has been linked to the nature of the dislocation cores themselves, suggesting that they might behave like 1D Lüttinger-liquid systems promoting mass flux across a network of superfluid dislocation cores [10, 11, 14–16].

Despite their prominent role in the interpretation of these experiments, however, our knowledge regarding the most fundamental properties of dislocations in hcp ^{4}He remains far from complete. For instance, although plastic deformation is known to occur predominantly on the basal plane [4, 17], there is no direct experimental insight into their fundamental core structure and mobility. In this context, atomistic modeling techniques provide useful tools to extract such characteristics in a systematic fashion [18]. However, for the case of hcp ^{4}He, except for a set of calculations based on a variational Jastrow-type wavefunction [19], fully atomistic studies have remained limited to dislocations with Burgers vectors aligned with the c-axis [14, 15], which are not expected to play a significant role in the mechanical behavior of hcp ^{4}He [17, 20–22].

In this Letter we present an atomistic study of the edge and screw dislocations with Burgers vectors in the basal plane, investigating the fundamental structure of their cores as well as the lattice resistance opposing their motion. The basic computational framework is the path-integral Monte Carlo (PIMC) method [23–26], which has been the standard tool for atomistic the study of the condensed phases of ^{4}He [14, 27–33]. First, our results clearly establish that basal-plane dislocations in hcp ^{4}He are dissociated into nonsuperfluid Shockley partial dislocations separated by an area of stacking fault (SF) and suggests that these dislocation cores are unlikely to play a role in the proposed superfluid-core interpretation of the mass flow experiments mentioned above. Furthermore, we find the partial dislocation cores to be extremely mobile, with their centroid positions fluctuating significantly compared to the periodicity of the lattice perpendicular to the dislocation lines, even in the absence of driving stresses. This finding is consistent with the experimental reports on giant plasticity and our results suggest that, in addition to the structural characteristics of the partial dislocations, zero-point effects play a role in this phenomenon.

Our calculations are based on fully periodic cells containing a dipole of screw/edge dislocations with opposite Burgers vectors. The atomic configurations were prepared from an initially defect-free crystal by introducing atomic displacements according to the linear elastic solutions for the strain fields associated with both dislocation characters [12, 18]. To minimize the effect of periodic image forces perpendicular to the basal plane [18], the two dislocations of the dipole are placed on basal planes at a distance equal to half the box height along the [0001] direction, as shown for the screw dipole in Fig. 1a). The corresponding cells contain 8064 and 7056 atoms for the screw and edge, respectively, at a molar volume of 21 cm^3, for which the Burgers vector magnitude is ~ 3.66 Å. Equilibration of the systems was carried out using by sampling atomic and cell configurations us-

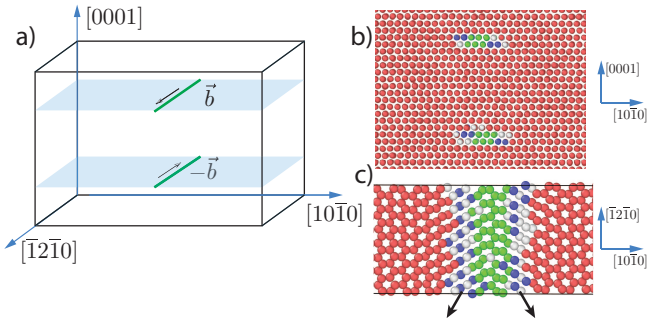

Figure 1. (Color online) a) Cell geometry with two screws of opposite Burgers vectors placed on basal planes separated by half the box height along the [0001] direction. b) Path centroid positions after PIMC relaxation viewed along the [$\bar{1}$2$\bar{1}$0]. Colors represent ranges of common-neighbor analysis (see text). Red and green depict hcp and fcc-type atomic environments, respectively. c) Centroids of two atomic planes containing one of the dislocations. Green area represents SF. Arrows depict partial dislocation Burgers vectors.

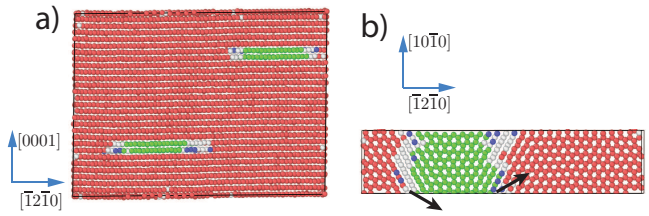

Figure 2. (Color online) Configuration for the edge dislocation after PIMC relaxation. Colors represent ranges of the common-neighbor parameter (see text). Red and green depict hcp and fcc-type atomic environments, respectively. a) Path centroid positions viewed along the [10$\bar{1}$0] direction. b) Centroids of two atomic planes containing one of the dislocations. Green area represents SF area and arrows depict partial dislocation Burgers vectors.

ing the isothermal-isostress ensemble approach [34] implemented in the `PIMC++` package [25]. We employ an imaginary time step of $\tau = 1/40\ K^{-1}$ and a path discretization in terms of 150 time slices, which corresponds to a temperature of $T = 0.267\ K$. Previous PIMC studies of the mechanical behavior of hcp ^{4}He have shown that this time step provides reliable results [32, 33]. A pair action based on the Aziz [40] pair potential was used. Only hydrostatic pressure (i.e., no shear components) was applied to the maintain an average molar volume of 21 cm^3. To analyze the atomic structures, path configurations are stored after every 250th bisection move in the PIMC runs. Permutation sampling was initially disabled to reduce the computational effort associated with the equilibration stage of the dislocation geometries but it was invoked during a number of subsequent runs to assess possible effects associated with Bose-Einstein statistics.

Figs. 1 b) and c) depict representative equilibrated path-centroid configurations for the screw dipole cell. Each atom is colored according to its common-neighbor order-parameter value [41, 42], which distinguishes between different atomic coordination levels. Red and green depict atoms in hcp and fcc regions, respectively, whereas the other colors indicate intermediate coordinations. The images clearly reveal the dissociation of the perfect screw dislocation into two 30° Shockley partials [12, 13], with their cores shown as the light blue and white circles, separated by a ribbon of SF depicted in green. Subsequent runs including permutation sampling reveal that these partial cores do not exhibit any sign of superfluidity given the absence of persisting permutation cycles. Analogous dissociation also occurs for the edge dislocation as shown in Fig. 2, with the perfect dislocation splitting up into two 60° non-superfluid Shockley partials joined by an area of SF. This area is wider than that for the screw dislocation case, however, because of the larger edge component of the 60° partials [12, 13]. On the other hand, the dissimilar equilibrium arrangements observed for the screw and edge dipoles, with the former aligned vertically and the latter set in an oblique pattern, are a consequence of the different image stresses that occur in both cases due to the periodic boundary conditions [34]. While vanishing in the respective equilibrium configurations, these image stresses give rise to restoring forces for dislocation configurations that deviate from them [43]. In the absence of such image stresses, the equilibrium dissociation widths of isolated screw and edge dislocations are expected to be 81 and 434 Å, respectively, as discussed in the Supplemental Material [34]. This implies that basal-plane glide dislocations in hcp ^{4}He are effectively two-dimensional defect structures bounded by non-superfluid Shockley partial dislocations and indicates that the interpretation of recent mass flow experiments in terms of a network of 1D Lüttinger-liquid systems in the form of superfluid dislocation cores [10, 11, 14–16] does not involve basal-plane dislocations.

To analyze the dislocation core structure and mobility in more detail we first examine the path-centroid configurations in terms of a disregistry analysis of the relative displacement between the two atomic planes adjacent to the slip plane, tracking its progress along the direction perpendicular to the dislocation line. This is depicted in Fig. 3a), which shows a typical example of this analysis for a centroid snapshot obtained for the screw dislocation cell. The circles and dots depict the atoms in the layers immediately above and below the slip plane, respectively. The screw component of the disregistry is then monitored by measuring the vertical (i.e., screw) displacement of the dots with respect to their enclosing triangles (formed by circles) along each of the 8 horizontal rows of such triangles. For each of these rows we then extract dislocation-core parameters such as position and core width by fitting the disregistry profile to the Peierls-Nabarro (PN) model [12, 18], which, for the dislocations

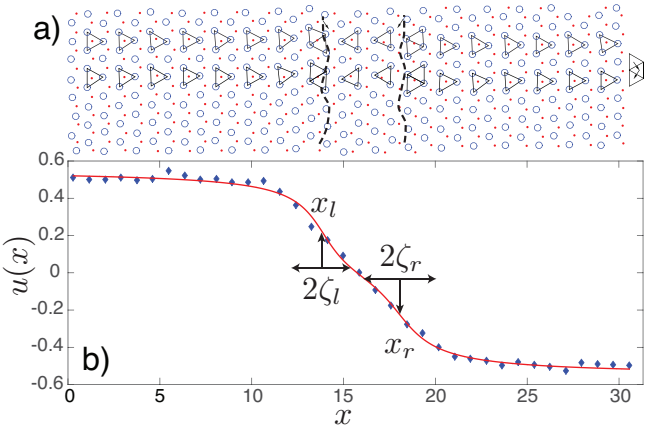

Figure 3. (Color online) Disregistry analysis for screw dislocation configuration. a) Atoms in layers immediately below (circles) and above (dots) slip plane. Screw disregistry is measured by monitoring the vertical position of dot with respect to its enclosing triangle along 8 horizontal rows of triangles (two shown). Dashed lines depict spline fits through set of 8 core positions as determined from fits to the PN model. b) Representative fit of PIMC data for the disregistry u (diamonds, in units of the full Burgers vector b) as a function of horizontal position x (also in units of b) to the PN-model of Eq. 1 (red line). Corresponding partial dislocation positions (x_l, x_r) and core widths ($2\,\zeta_l$, $2\,\zeta_r$) are also marked.

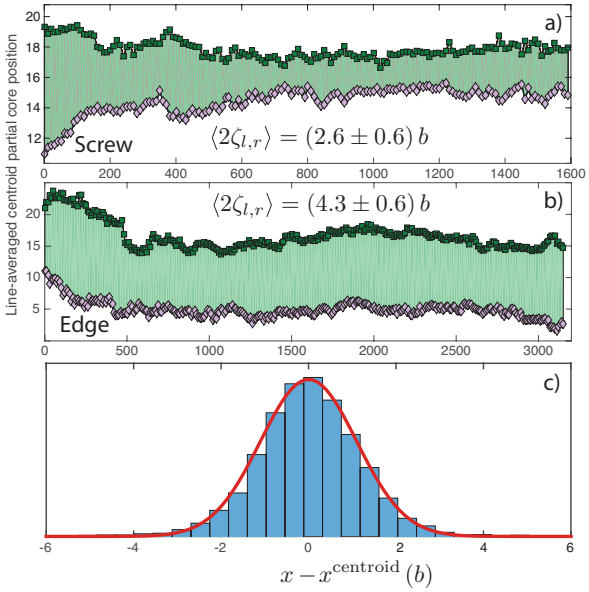

Figure 4. (Color online) a) and b) Centroid core positions for the left (diamonds) and right (squares) partial dislocations of the dissociated screw and edge dislocations as a function of PIMC snapshot number. Vertical axes are in units of the perfect Burgers vector b. Shaded areas between partial positions denote SF widths. Mean partial dislocation core widths are also indicated. Mean confidence intervals for PN fits of the partial positions are $\sim \pm 0.3b$ and $\sim \pm 0.4b$ for the screw and edge dislocations respectively. c) Histogram of partial core positions relative to centroid partial core position as determined by fitting PN expression to 50 displacement profiles per PIMC snapshot, each obtained from an average over 3 consecutive time slices.

considered here, takes the form

$$u(x) = \frac{c}{\pi}\left(\tan^{-1}\left[\frac{x - x_l}{\zeta_l}\right] + \tan^{-1}\left[\frac{x - x_r}{\zeta_r}\right]\right), \qquad (1)$$

with x_l and x_r the positions of the left and right partials, respectively, ζ_l and ζ_r the half-widths of both cores, and c an amplitude parameter. A representative fit of this kind is shown in Fig. 3b).

The dashed lines in Fig. 3a) are splines through the set of 8 core positions obtained from such PN-model fits and serve as guides to the eye identifying both partial dislocation lines. We find the centroid line fluctuations to be small in all studied configurations, with their amplitude being of the same order of magnitude as the confidence intervals in the core positions parameters as determined from the regression process. Therefore, in our further analysis we will describe the core parameters in terms of their mean values as obtained by averaging them over the 8 core positions along each partial dislocation line.

Fig. 4 displays the evolution along the PIMC simulations of the line-averaged centroid partial core positions for the lower screw and edge dislocations of Figs. 1 b) and 2 a), respectively. After an initial transient, both dislocation configurations are seen to attain their equilibrium structures in which the centroid positions of the partials become stationary and the SF widths equilibrate at mean values of $(2.6 \pm 0.1)\,b$, and $(11.4 \pm 0.1)\,b$ for the screw and edge dislocations, respectively. Despite the stationary character of the centroid core positions, however, they are observed to fluctuate substantially, displaying digressions of $\sim 1.9\,b$ and $\sim 4.5\,b$ along the $[10\bar{1}0]$ and $[\bar{1}2\bar{1}0]$ directions for the screw and edge dislocations, respectively. The fact that the magnitude of these fluctuations is more than twice as large as the lattice periodicities perpendicular to the dislocation lines ($\frac{1}{2}\sqrt{3}\,b$ and b for the screw and edge dislocations, respectively) and given that these occur in the absence of driving stresses and the presence of restoring image forces represent a clear indication of an effectively vanishing lattice resistance to dislocation motion. From a structural point of view, the elevated dislocation mobility is consistent with the diffuse character of the 30° and 60° partial dislocation cores, with their total displacement spread out across several (~ 3 and 4, respectively) atomic rows. Indeed, in classical crystals such planar and rather wide cores with a partial Burgers vector are known to experience very low lattice resistance to their motion [44].

In the case of dislocations in a quantum crystal such as hcp ^{4}He an additional question of relevance is whether or not quantum-mechanical zero-point effects, known to be substantial in this system, may also affect dislocation mobility. Indeed, even in classical metals such effects have

been shown to play a role under certain conditions [45]. In PIMC simulations the finite extent of the ring polymers represented by the imaginary time slices encodes the quantum-mechanical uncertainty in the atomic positions in the system. Given that these observables also characterize the dislocation core location through the parameters x_l and x_r in the PN model it seems plausible that the atomic zero-point fluctuations may also give rise to an intrinsic quantum-mechanical uncertainty in the dislocation core position. To assess the possible magnitude of such uncertainties, we analyze the statistics of the PN disregistry profiles corresponding to the set of 150 time slices that constitute the cyclic polymers for each PIMC snapshot. To this end, we construct histograms that record dislocation core position samples relative to the centroid core location for the PIMC snapshot under consideration, by fitting the PN expression to disregistry profiles obtained by averaging over small groups of consecutive time slices. Fig. 4 c) shows a typical histogram of this kind for the 60° partial, determined by fitting the PN expression to 50 disregistry profiles, each computed by averaging over 3 consecutive time slices for a given PIMC configuration and repeating this analysis for a set of 200 PIMC snapshots after reaching the stationary state. In view of the large atomic zero-point fluctuations in hcp ^{4}He, which lead to disordered-like patterns for single-slice configurations, the motivation for using averages over 3 time slices is that this number is sufficiently large to discern the crystallinity of the system and enable characterization of the dislocation configurations (i.e., giving PN fits with a root-mean-square error smaller than 15 %), yet small enough to appreciate the magnitude of the intrinsic zero-point fluctuations of the dislocation parameters.

The distribution is approximately Gaussian with a standard deviation of $\sim 1.1\,b$, which is of the order of the distance between two adjacent lattice rows that can host the partial dislocation core. This suggests that the intrinsic variations in the partial core position due to the zero-point fluctuations of the ^{4}He atoms are in fact appreciable, with different groups of time slices describing the core position of the dislocation at distinct lattice positions. Not only does this observation highlight the intrinsic quantum uncertainty in the position of the dislocation line at low temperatures, it also suggests that, in absence of significant thermal agitation, the zero-point fluctuations effectively eliminate any resistance to the dislocation's motion, with the defect being essentially free to move through the lattice.

In summary, we have carried out a PIMC study into the structure and mobility of basal-plane dislocations in hcp ^{4}He. Our results clearly establish that basal-plane dislocations in hcp ^{4}He are dissociated into nonsuperfluid Shockley partial dislocations separated by areas of stacking fault (SF). This indicates that these dislocation cores are unlikely to be involved in the proposed superfluid-core interpretation of recent mass flow experiments [10, 11, 14–16]. Furthermore, we find the intrinsic lattice resistance to basal-plane dislocation motion to be effectively vanishing, with the dislocation lines fluctuating across substantial distances even in the absence of driving stresses. This is consistent with the experimental observations of giant plasticity [4–6] in the basal plane and, in addition to the wide character of the partial dislocation cores, our results suggest that zero-point fluctuations play a central role in this phenomenon.

ACKNOWLEDGMENTS

E.J.L.B. and M.K. gratefully acknowledge support from the Brazilian agencies CNPq, Fapesp, and Capes. M.K. acknowledges support from the Center for Computational Engineering and Sciences - Fapesp/Cepid no. 2013/08293-7. This work was partially supported by the U.S. Department of Energy, Office of Basic Energy Sciences, Division of Materials Sciences and Engineering under Award No. DE-SC0010412 (W.C.). This work was supported in part by the U.S. Department of Energy at the Lawrence Livermore National Laboratory under Contract DE-AC52-07NA27344.

* landinezbord1@llnl.gov
† caiwei@stanford.edu
‡ dekoning@ifi.unicamp.br

[1] E. Kim and M. H. W. Chan, Nature **427**, 225 (2004).
[2] E. Kim and M. H. W. Chan, Science **305**, 1941 (2004).
[3] D. Y. Kim and M. H. W. Chan, Phys. Rev. Lett. **109**, 155301 (2012).
[4] A. Haziot, X. Rojas, A. D. Fefferman, J. R. Beamish, and S. Balibar, Phys. Rev. Lett. **110**, 035301 (2013).
[5] C. Zhou, C. Reichhardt, M. J. Graf, J.-J. Su, A. V. Balatsky, and I. J. Beyerlein, Phys. Rev. Lett. **111**, 119601 (2013).
[6] A. Haziot, X. Rojas, A. D. Fefferman, J. R. Beamish, and S. Balibar, Phys. Rev. Lett. **111**, 119602 (2013).
[7] M. W. Ray and R. B. Hallock, Phys. Rev. Lett. **100**, 235301 (2008).
[8] M. W. Ray and R. B. Hallock, Phys. Rev. B **79**, 224302 (2009).
[9] M. W. Ray and R. B. Hallock, Phys. Rev. B **84**, 144512 (2011).
[10] Y. Vekhov, W. Mullin, and R. Hallock, Phys. Rev. Lett. **113**, 035302 (2014).
[11] Y. Vekhov and R. B. Hallock, Phys. Rev. B **90**, 134511 (2014).
[12] J. P. Hirth and J. Lothe, *Theory of Dislocations*, 2nd ed. (Krieger Publishing Company, 1992).
[13] D. Hull and D. Bacon, *Introduction to dislocations* (Butterworth-Heinemann, 2001).
[14] M. Boninsegni, A. B. Kuklov, L. Pollet, N. V. Prokof'ev, B. V. Svistunov, and M. Troyer, Phys. Rev. Lett. **99**, 035301 (2007).

[15] S. G. Söyler, A. B. Kuklov, L. Pollet, N. V. Prokof'ev, and B. V. Svistunov, Phys. Rev. Lett. **103**, 175301 (2009).

[16] A. B. Kuklov, L. Pollet, N. V. Prokof'ev, and B. V. Svistunov, Phys. Rev. B **90**, 184508 (2014).

[17] M. A. Paalanen, D. J. Bishop, and H. W. Dail, Phys. Rev. Lett. **46**, 664 (1981).

[18] V. V. Bulatov and W. Cai, *Computer simulations of dislocations* (Oxford University Press, 2006).

[19] R. Pessoa, S. A. Vitiello, and M. de Koning, Phys. Rev. Lett. **104**, 085301 (2010).

[20] Y. Hiki and F. Tsuruoka, Phys. Lett. A **56**, 484 (1976).

[21] Y. Hiki and F. Tsuruoka, Phys. Lett. A **62**, 50 (1977).

[22] F. Tsuruoka and Y. Hiki, Phys. Rev. B **20**, 2702 (1979).

[23] D. M. Ceperley, Rev. Mod. Phys. **67**, 279 (1995).

[24] D. M. Ceperley and B. Bernu, Phys. Rev. Lett. **93**, 155303 (2004).

[25] B. K. Clark and D. M. Ceperley, Comput. Phys. Commun. **179**, 82 (2008).

[26] W. Krauth, *Statistical Mechanics: Algorithms and Computations* (Oxford University Press, Oxford, 2006).

[27] M. Boninsegni, A. B. Kuklov, L. Pollet, N. V. Prokof'ev, B. V. Svistunov, and M. Troyer, Phys. Rev. Lett. **97**, 080401 (2006).

[28] M. Boninsegni, N. Prokof'ev, and B. Svistunov, Phys. Rev. Lett. **96**, 105301 (2006).

[29] L. Pollet, M. Boninsegni, A. B. Kuklov, N. V. Prokof'ev, B. V. Svistunov, and M. Troyer, Phys. Rev. Lett. **98**, 135301 (2007).

[30] L. Pollet, M. Boninsegni, A. B. Kuklov, N. V. Prokof'ev, B. V. Svistunov, and M. Troyer, Phys. Rev. Lett. **101**, 097202 (2008).

[31] P. Corboz, L. Pollet, N. V. Prokof'ev, and M. Troyer, Phys. Rev. Lett. **101**, 155302 (2008).

[32] L. A. P. Ardila, S. A. Vitiello, and M. de Koning, Phys. Rev. B **84**, 094119 (2011).

[33] E. J. L. Borda, W. Cai, and M. de Koning, Phys. Rev. Lett. **112**, 155303 (2014).

[34] For further details, see Supplemental Material which includes Refs. [35-39].

[35] M. Parrinello and A. Rahman, J. Appl. Phys. **52**, 7182 (1981).

[36] M. Parrinello and A. Rahman, J. Chem. Phys. **76**, 2662 (1982).

[37] M. E. Tuckerman, *Statistical Mechanics: Theory and Molecular Simulation* (Oxford University Press, Oxford, 2010).

[38] R. Najafabadi and S. Yip, Scr. Metall. **17**, 1199 (1983).

[39] W. P. Kuykendall and W. Cai, Model. Simul. Mater. Sci. Eng. **21**, 055003 (2013).

[40] R. A. Aziz, A. R. Janzen, and M. R. Moldover, Phys. Rev. Lett. **74**, 1586 (1995).

[41] J. D. Honeycutt and H. C. Andersen, J. Phys. Chem. **91**, 4950 (1987).

[42] A. Stukowski, Model. Simul. Mater. Sci. Eng. **18**, 015012 (2010).

[43] W. Cai, V. V. Bulatov, J. Chang, J. Li, and S. Yip, Philos. Mag. **83**, 539 (2003).

[44] W. Cai, V. V. Bulatov, J. Chang, J. Li, and S. Yip, in *Dislocations in Solids*, Dislocations in Solids, Vol. 12, edited by F. Nabarro and J. Hirth (Elsevier Science, 2004) Chap. 64, p. 1.

[45] L. Proville, D. Rodney, and M.-C. Marinica, Nat. Mater. **11**, 845 (2012).